Table 1 Summary of clinical features of 22 patients

Age (years)			CT			PTA		Vertigo	Thyroid	
			EVA	MD	VE	HL (dB)	Conductive hearing loss		Goiter	Thyroid function
1	3	R	+	+	+	SO	unknown	-	-	normal
		L	+	+	+	SO	unknown			
2	14	R	+	+	-	105	+	-	+	normal
		L	+	+	-	96	+			
3	21	R	+	+	+	73	+	+	+	normal
		L	+	+	+	91	+			
4	21	R	+	-	-	81	+	+	+	normal
		L	+	-	-	85	+			
5	28	R	+	+	+	96	+	+	+	normal
		L	+	+	+	SO	+			
6	33	R	+	+	-	101	+	+	+	normal
		L	+	+	+	106	+			
7	1	R	+	+	-	SO	unknown	-	-	normal
		L	+	+	+	SO	unknown			
8	1	R	+	-	-	SO	unknown	-	-	normal
		L	+	-	-	103	unknown			
9	2	R	+	+	-	101	unknown	-	-	normal
		L	+	+	-	100	unknown			
10	12	R	+	-	-	95	+	-	+	normal
		L	+	-	-	100	+			
11	29	R	+	+	+	85	+	-	-	
		L	+	+	+	110	+			
12	0	R	+	-	-	55	unknown	+	-	normal
		L	+	-	-	73	unknown			
13	3	R	+	-	+	85	unknown	+	-	normal
		L	+	+	+	58	+			
14	5	R	+	+	+	95	+	+	-	normal
		L	+	+	+	93	+			
15	5	R	+	+	+	103	+	-	-	normal
		L	+	+	+	100	unknown			
16	6	R	+	-	-	81	+	+	-	normal
		L	+	-	-	91	+			
17	7	R	+	-	-	83	+	-	-	normal
		L	+	-	+	81	+			
18	14	R	+	+	+	96	+	-	+	normal
		L	+	+	+	91	+			
19	16	R	+	-	+	91	+	-	+	normal
		L	-	-	+	21	-			
20	26	R	+	-	-	98	+	+	-	normal
		L	+	-	+	103	+			
21	5	R	+	+	+	85	+	-	-	normal
		L	+	+	-	97	+			
22	10	R	+	-	-	53	+	-	-	normal
		L	-	-	-	15	-			

EVA enlarged vestibular aqueduct, *MD* Mondini malformation, *VE* vestibular enlargement, *PTA* pure tone audiogram, *HL* hearing level, *SO* scale out, *NA* no available data.

Table 2 Primer sequences used for nested real-time PCR

Nested PCR assay			Sequence	PCR product size (bp)
First-step PCR (external primer)	Exon 14	forward	TCTTGGAATGGCCTTGGAAGC	282
	Exon 17	reverse	TGAAACAGCATCACTTATGATGC	
Second-step PCR (internal primer)	Exon 15	forward	TGAAGAACCTCAAGGAGTGAAG	154
	Exon 16	reverse	TTTCTGTATTTTCCTCAGCGCT	

reaction volume was adjusted to 20 μl with distilled H_2O. A Light Cycler real-time quantitative PCR system (Roche, Basel Switzerland) was used for amplification and detection of the PCR products. A 40 step cycle of thermal cycler program was performed as follows: denaturation at 95°C for 5 min; 40 cycles of 95°C for 10 s, 60°C for 20 s, and 72°C for 40 s; followed by recording the fluorescence values after each elongation step and melting curve analysis with denaturation at 95°C for 5 s, annealing at 65°C for 1 min, and redenaturation by increasing the temperature to 95°C. The second-step PCR products were separated by 1.5% agarose gel electrophoresis, stained with ethidium bromide, and visualized by UV transillumination. For this analysis, we used three control subjects with no mutations (wild type), three patients compound heterozygous for IVS15 + 5G > A/H723R, and three patients homozygous for IVS15 + 5G > A.

Validation of comparative CT ($2^{-\Delta\Delta CT}$) method and calculations for quantifying *SLC26A4* mRNA

We used the CT ($2^{-\Delta\Delta CT}$) method by assuming approximately equal amplification efficiencies for both target and reference genes. This prerequisite was verified by performing a validation experiment using both *SLC26A4* and a housekeeping gene. Calculations were made using the comparative CT ($2^{-\Delta\Delta CT}$) method. *GAPDH* (glyceraldehyde 3-phosphate dehydrogenase), *PGK-1* (phosphoglycerate kinase 1), and *ACTB* (actin beta) were used as internal reference genes for PCR normalization with regard to the amount of RNA added to the reverse transcription reactions. Normalized results were expressed as the mean ratio of *SLC26A4* mRNA to *GAPDH* mRNA, *PGK-1* mRNA, and *ACTB* mRNA. To evaluate relative transcript levels, the threshold cycle value (Ct) of each sample was used to calculate and compare the ΔCt of each sample to that of the control subject and patients with a compound heterozygous for IVS15 + 5G > A/H723R, and a homozygous for IVS15 + 5G > A. ΔΔCT was also calculated to compare the transcript levels in the control subject, and patients with a compound heterozygous for IVS15 + 5G > A/H723R, and a homozygous for IVS15 + 5G > A. The transcript levels were calculated in each genotype with three subjects and each subject was calculated in triplicate.

Results

Mutation analysis for *SLC26A4*

By direct DNA sequence analysis, *SLC26A4* mutations were observed in 21 of 22 patients. Among the 21 patients with mutations, a compound heterozygous mutation for IVS15 + 5G > A/H723R was identified in nine patients (Figure 3C, D), a homozygous mutation for H723R was identified in five patients (Figure 3E), and a homozygous substitution of IVS15 + 5G > A was identified in six patients (Figure 3F). A compound heterozygous substitutions for IVS15 + 5G > A/T527P was identified in one subject. We could not identify any *SLC26A4* mutations in one subject (Table 3). We could not find the substitution IVS15 + 5G > A in 100 control objects.

Clinical characteristics

Table 1 summarizes the clinical characteristics of all 22 subjects. High-resolution temporal bone CT scans revealed that bilateral EVA was present in 20 patients and unilateral EVA was present in other two. Mondini dysplasia and vestibular enlargement was observed in 17 ears (17/44; 39%) and 22 ears (22/44; 50%), respectively.

Hearing loss grades in the affected ears ranged from moderate to profound in the patients with EVA (Table 1). The hearing levels of the two unaffected ears were normal and mild hearing loss, respectively. Table 4 shows the hearing level distributions based on genotypes. No significant differences were expected in the distributions for hearing level among the five genotype groups due to the small sample of only 22 patients.

Neck examinations revealed thyroid goiters in 8 of 22 patients. Overall, 0% (0/11) and 73% (8/11) of the patients younger and older than 10 years of age, respectively, had a thyroid goiter. Their serum FT4 and TSH levels were within the normal ranges. There is no relation between occurrence of goiter and mutation genotypes.

SLC26A4 expression in patients with IVS15 + 5G > A

Electrophoretic separation of the real-time PCR products did not exhibit any bands in patients with the homozygous substitution for IVS15 + 5G > A (Figure 4C).

Because the *SLC26A4* expression levels were not high in blood samples, we investigated its expression using nested real-time qPCR for three control subjects, three

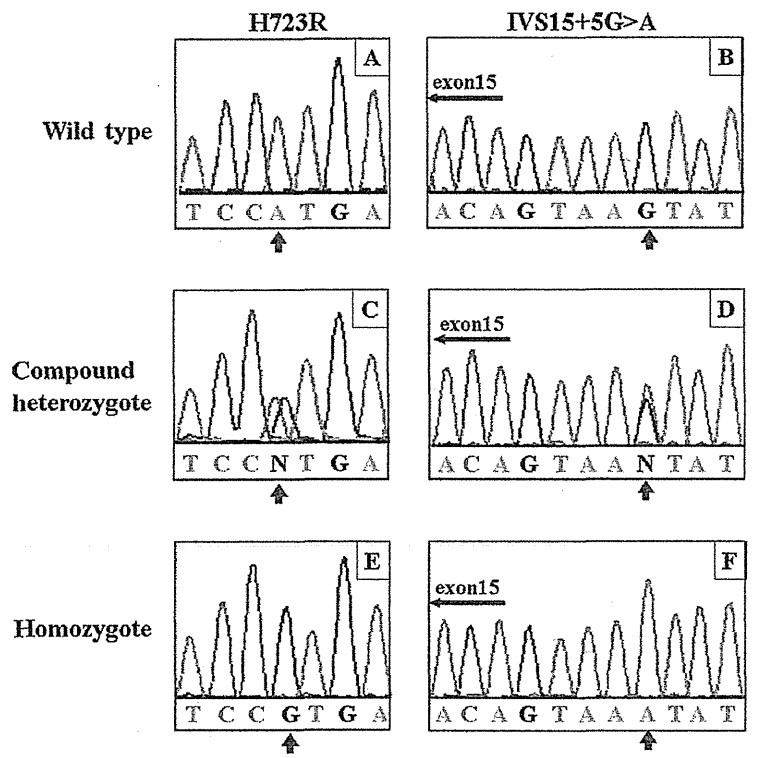

Figure 3 Examples of direct sequence analysis of the *SLC26A4* gene. Representative results of H723R and the IVS15 + 5G > A mutation analysis are shown. Genomic sequences of the *SLC26A4* gene in normal individuals (**A**), (**B**). A compound heterozygous mutation for IVS15 + 5G > A/H723R (**C**), (**D**). A homozygous mutation for H723R (**E**). A homozygous substitution of IVS15 + 5G > A (**F**). The arrows indicate the variant nucleotide.

patients with the compound heterozygous mutation for IVS15 + 5G > A/H723R, and three patients with the homozygous substitution for IVS15 + 5G > A. The control subjects had normal hearing without any malformations of the inner or middle ear and no family history of hearing loss. After obtaining a written informed consent, blood samples were collected from each subject and were subjected to Real-time PCR with SYBR Green and the expression level was evaluated using the comparative CT ($2^{-\Delta\Delta CT}$) method. The relative *SLC26A4* expression levels in the control no.1, control no.2 and control no.3 with no *SLC26A4* mutations were 9089 ± 441.5 (standard deviation), 2417 ± 189.5, and 4956 ± 260.4 respectively. In patient no.12, patient no.14 and patient no.16 with a compound heterozygous mutation for IVS15 + 5G > A/H723R were 979.5 ± 79.12, 2846 ± 206.5 and 1183 ± 33.93 respectively. In patient no.1, patient no.2 and patient no.4 with a homozygous substitution for IVS15 + 5G > A were $1.96 \times 10^{-4} \pm 7.66 \times 10^{-5}$, $5.76 \times 10^{-5} \pm 3.37 \times 10^{-6}$ and $4.35 \times 10^{-5} \pm 8.09 \times 10^{-6}$ respectively (Figure 5).

Based on the results of both electrophoresis and RT-nested qPCR, no *SLC26A4* expression was observed in patients with homozygous substitution of IVS15 + 5G > A.

Discussion

Correlations between *SLC26A4* genotypes and hearing phenotypes

Hearing loss in patients with EVA and PS is usually apparent at the pre- or perilingual stage [6,21]. Hearing loss in EVA and PS is sensorineural with some mixed hearing loss in the low-frequency range [22-27]. The hearing level sometimes deteriorates suddenly and may be followed by a partial recovery, such as with fluctuating hearing loss [28,29]. In our study, hearing loss was detected at the pre- or perilingual stage in all cases except for two cases of unilateral EVA. However, in all cases, hearing levels eventually deteriorated to severe or profound loss (Table 1) and were permanent with or without hearing fluctuation or stepwise hearing deterioration. No significant differences were observed in the hearing levels among the five genotypes (Table 4).

Correlations between *SLC26A4* genotypes and thyroid phenotype

SLC26A4 encodes for the 86 kDa transmembrane protein pendrin [7,30]. In the thyroid, this protein acts as co-transporter of chloride and iodine in the thyroid

Table 3 Distribution of *SLC26A4* genotypes of 22 patients

	Age at onset of hearing loss (years)	Age at genetic test (years)	Sex	Allele 1	Allele 2
1	0	3	M	IVS15 + 5G > A	IVS15 + 5G > A
2	2	14	F	IVS15 + 5G > A	IVS15 + 5G > A
3	3	21	F	IVS15 + 5G > A	IVS15 + 5G > A
4	2	22	F	IVS15 + 5G > A	IVS15 + 5G > A
5	0	23	M	IVS15 + 5G > A	IVS15 + 5G > A
6	0	29	F	IVS15 + 5G > A	IVS15 + 5G > A
7	0	1	F	H723R	H723R
8	1	1	F	H723R	H723R
9	4	2	M	H723R	H723R
10	0	12	F	H723R	H723R
11	5	29	M	H723R	H723R
12	0	0	M	IVS15 + 5G > A	H723R
13	2	3	M	IVS15 + 5G > A	H723R
14	0	5	F	IVS15 + 5G > A	H723R
15	1	5	F	IVS15 + 5G > A	H723R
16	0	6	F	IVS15 + 5G > A	H723R
17	2	7	F	IVS15 + 5G > A	H723R
18	2	14	F	IVS15 + 5G > A	H723R
19	7	16	F	IVS15 + 5G > A	H723R
20	5	26	M	IVS15 + 5G > A	H723R
21	1	5	M	H723R	T527P
22	7	10	F	ND	ND

ND not determined.

[31,32]. In PS patients, a mutation in *SLC26A4* results in reduced pendrin-induced chloride and iodide transport and, ultimately, goiter [33].

Goiter usually develops around the end of the first decade of life or during young adulthood, although the time of onset and severity vary considerably among patients [12,34], and even within families [35]. Despite an impaired incorporation of iodide, most patients with PS are clinically and biochemically euthyroid [21,34,36].

To our knowledge, no previous studies have investigated correlations between *SLC26A4* genotypes and the thyroid phenotype. In the present study, PS was diagnosed in 8 of 11 patients older than 10 years of age, but not in any of the 11 patients who were younger than 10 years of age. This indicates that it is difficult to diagnose PS before the age of 10 years.

Thyroid function was normal in all of the 21 patients we examined, as demonstrated by their normal serum concentrations of FT4 and TSH. There were no significant differences in serologic thyroid test results and goiter status among patients with homozygous substitution for IVS15 + 5G > A, the H723R homozygous mutation, or compound heterozygous mutation for IVS15 + 5G > A/H723R. Therefore, our results indicate that serologic testing of FT4 and TSH levels is not useful to distinguish between individuals with PS or EVA.

Distributions of *SLC26A4* mutations in EVA and PS patients in Okinawa Islands

It was previously reported that the spectrum of *SLC26A4* mutations varied based on ethnic background [35,36]. H723R and IVS7-2A > G are prevalent alleles that account for the majority of the observed *SLC26A4* mutations in East Asian populations [35]. In the Japanese population, H723R was the most common mutation [15,36,37]. In Chinese and Taiwanese populations, IVS7-2A > G was the most common mutation [38-40], whereas in the Korean population, H723R and IVS7-2A > G were the most frequent and accounted for 60.2% (47/78) and 30.7% (24/78) of the mutated alleles, respectively [41].

Ancestral differences have been reported between people from Okinawa Islands and those from the main islands of Japan based on single-nucleotide polymorphism genotypes [16]. We analyzed *SLC26A4* mutations among 22 patients with EVA or PS from 21 unrelated families. H723R have been reported as the most common mutation found in the main islands of Japan. As with H723R mutation, IVS15 + 5G > A substitution was

Table 4 Clinical features in different genotype groups

Genotype	Hearing level					CT		Vertigo
	Normal	Mild	Moderate	Severe	Profound	MD	VE	
IVS15 + 5 G > A homozygous (n = 6)	0	0	0	3	9	6/12	6/12	4/6
H723R homozygous (n = 5)	0	0	0	1	9	4/10	3/10	0/5
IVS15 + 5 G > A/H723R (n = 9)	0	1	2	4	11	5/18	11/18	4/9
IVS15 + 5G > /T527P (n = 1)	0	0	0	1	1	2/2	1/2	0/1
No mutation (n = 1)	1	0	1	0	0	0/2	0/2	0/1
Subtotal	1	1	3	9	30	17/44	21/44	8/22
Total			44					

Normal: ≤20 dB; Mild: 21–40 dB; Moderate: 41–70 dB; Severe: 71–90 dB; Profound: >91 dB.
MD Mondini malformation, *VE* Vestibular enlargement, *CT* computed tomography.

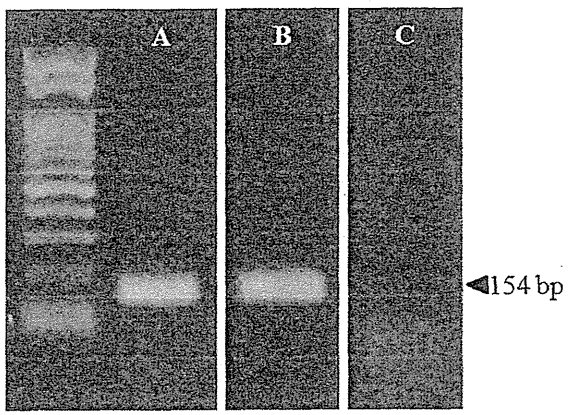

Figure 4 Expression of the *SLC26A4* gene in patients with PS or EVA. The expected RT-nested PCR amplification product of *SLC26A4* was 154 base pairs (bp) in length. Agarose gel electrophoresis shows the 154 bp band for the control subject (**A**) and the patient with IVS15 + 5G > A/H723R compound heterozygous mutation (**B**); however, there was no band for the patient with IVS15 + 5G > A homozygous substitution (**C**).

also identified most frequently in 15 of 22 of our Okinawa patients. The substitution of IVS15 + 5G > A in one allele have been reported only 10 cases in Asian populations [36,42-45]. Thus, IVS15 + 5G > A was the characteristic *SLC26A4* gene mutation among patients in Okinawa Islands, indicating a difference in the spectrum of *SLC26A4* mutations among patients in Okinawa Islands compared with patients in other

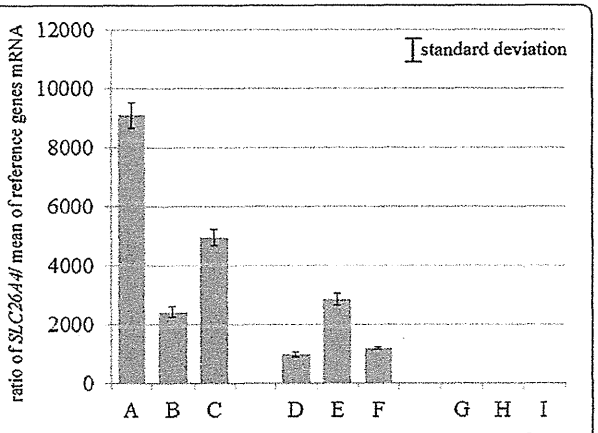

Figure 5 Relative expression of the *SLC26A4* gene in control subjects and in patients with a homozygous mutation of IVS15 + 5G > A or compound heterozygous mutation of IVS15 + 5G > A/H723R. The ratio of SLC26A4 mRNA to GAPDH mRNA is shown in three control subjects (**A, B, C**), three patients with compound heterozygous mutation of IVS15 + 5G > A/H723R (**D, E, F**), and three patients with IVS15 + 5G > A homozygous substitution (**G, H, I**). No expression of *SLC26A4* was observed in the three patients with the IVS15 + 5G > A homozygous substitution (**G, H, I**). All experiments were done in tripricate.

populations. These results suggest that this *SLC26A4* mutation may have originated from a common ancestor.

Pathogenic effect of IVS15 + 5G > A substitution

The heterozygous substitution of IVS15 + 5G > A has been assumed to cause aberrant splicing [36,42-45]. However, Yang et al. [42] could not find any abnormal RT-PCR products related to the size for SLC26A4 sequence analysis in patients with splice mutation. Because its pathogenicity was only implicated on the basis of uncommon polymorphisms, the pathogenic potential of IVS15 + 5G > A still remains unknown.

Substitutions near the canonical splice sites are difficult to classify as pathogenic or non-disease causing. Because such substitutions affect proper RNA splicing but some substitutions do not cause any effect [46-48]. Thus, it is important to determine the pathogenic effect of a particular substitution near the donor site by mRNA analysis [48]. We investigated *SLC26A4* expression in patients with compound heterozygous mutation for IVS15 + 5G > A/H723R and homozygous substitution for IVS15 + 5G > A by RT-PCR and RT-real time PCR by targeting genes around these mutations. No aberrant PCR products were detected in the patient with heterozygous substitution of IVS15 + 5G > A (Figure 4B), which suggests that IVS15 + 5G > A does not cause aberrant splicing, as also argued by Yang et al. However, in patients with the homozygous substitution of IVS15 + 5G > A, *SLC26A4* was not expressed, as shown in Figure 4. In addition, for patients with the heterozygous substitution, *SLC26A4* expression was reduced from the normal control level. These findings suggest that IVS15 + 5G > A disrupts pre-mRNA splicing and causes the loss of *SLC26A4* expression. The patients in Yang et al. [42] were heterozyote so that Yang et al. [42] most likely amplified the non-mutated allele. Taken together, our results indicate that the substitution of IVS15 + 5G > A is a loss-of-function mutation caused by a loss of *SLC26A4* expression.

Conclusions

We found no correlations between the type of *SLC26A4* mutation and hearing levels or the thyroid phenotype. Moreover, thyroid testing using serum FT4 and TSH levels was not useful for distinguishing between individuals with PS and EVA.

The substitution of IVS15 + 5G > A in the *SLC26A4* was unique and the most common in PS and EVA patients from Okinawa Islands. This supports that the spectrum of *SLC26A4* mutations differs by geographic area in East Asia. Our qPCR results for *SLC26A4* indicate that the substitution of IVS15 + 5G > A should be a pathogenic mutation that leads to a loss of *SLC26A4* expression and results in a phenotype of PS and EVA.

Competing interests
The authors declare that they have no competing interests.

Authors' contributions
AG diagnosed the patients, collected clinical data, performed the experiments, and wrote the manuscript. TK, KY, and SU carried out data analysis. KN, TT, and MS edited the manuscript and supervised the project. All authors read and approved the final manuscript.

Acknowledgements
This work was supported in part by the Japan Society for the Promotion of Science (JSPS) KAKENHI Grant-in-Aid for Young Scientists (B) Number 23791914, by Special Account Budget for Education and Research from the Japan Ministry of Education and by research grants from the Japan Ministry of Health, Labor, and Welfare.

Author details
[1]Department of Otorhinolaryngology-Head and Neck Surgery, University of the Ryukyus, Okinawa, Japan. [2]Department of Medical Genetics, University of the Ryukyus, Okinawa, Japan. [3]Department of Otorhinolaryngology-Head and Neck Surgery, University of Miyazaki, Miyazaki, Japan. [4]Department of Otorhinolaryngology, Shinshu University School of Medicine, Nagano, Japan.

Received: 18 January 2013 Accepted: 17 May 2013
Published: 24 May 2013

References

1. Downs MP: **Universal newborn hearing screening–the Colorado story.** *Int J Pediatr Otorhinolaryngol* 1995, **32**:257–259.
2. Mehl AL, Thomson V: **Newborn hearing screening: the great omission.** *Pediatrics* 1998, **101**:E4.
3. Mehl AL, Thomson V: **The Colorado newborn hearing screening project, 1992–1999: on the threshold of effective population-based universal newborn hearing screening.** *Pediatrics* 2002, **109**:E7.
4. Bitner-Glindzicz M: **Hereditary deafness and phenotyping in humans.** *Br Med Bull* 2002, **63**:73–94.
5. Morton NE: **Genetic epidemiogy of hearing impairment.** *Ann NY Acad Sci* 1991, **630**:16–31.
6. Pendred V: **Deaf-mutation and goiter.** *Lancet* 1896, **2**:532.
7. Everett L, Glaser B, Beck J, Idol J, Buchs A, Heyman M, Adawi F, Hazani E, Nassir E, Baxevanis A, Sheffield V, Green E: **Pendred syndrome is caused by mutations in a putative sulphate transporter gene (*PDS*).** *Nat Genet* 1997, **17**:411–422.
8. Li XC, Everett LA, Lalwani AK, Desmukh D, Friedman TB, Green ED, Wilcox ER: **A mutation in PDS causes non-syndromic recessive deafness.** *Nat Genet* 1998, **18**:215–217.
9. Johnsen T, Jørgensen MB, Johnsen S: **Mondini cochlea in Pendred's syndrome.** *Acta Otolaryngol* 1986, **102**:239–247.
10. Nakagawa O, Ito S, Hanyu O, Yamazaki M, Urushiyama M: **Female siblings with Pendred's syndrome.** *Int Med* 1994, **33**:369–372.
11. Reardon W, Trembath RC: **Pendred syndrome - 100 years of underascertainment?** *Q J Med* 1997, **90**:443–447.
12. Campbell C, Cucci RA, Prasad S, Green GE, Edeal JB, Galer CE, Karniski LP, Sheffield VC, Smith RJ: **Pendred syndrome, DFNB4, and PDS/SLC26A4 identification of eight novel mutation and possible genotype–phenotype correlations.** *Hum Mutat* 2001, **17**:404–411.
13. Usami S, Abe S, Weston MD, Shinkawa H, Camp GV, Kimberling WJ: **Non-syndromic hearing loss associated with enlarged vestibular aqueduct is caused by PDS mutations.** *Hum Genet* 1999, **104**:188–192.
14. Park HJ, Shaukat S, Liu XZ, Hahn SH, Naz S, Ghosh M, Kim HN, Moon SK, Abe S, Tsukamoto K, Riazuddin S, Kabra M, Erdenetungalag R, Radnaabazar J, Khan S, Pandya A, Usami S-I, Nance WE, Wilcox ER, Riazuddin S, Griffith AJ: **Origins and frequencies of SLC26A4 (PDS) mutations in east and south Asians: Global implications for the epidemiology of deafness.** *J Med Genet* 2003, **40**:242–248.
15. Tsukamoto K, Suzuki H, Harada D, Namba A, Abe S, Usami S: **Distribution and frequencies of PDS (SLC26A4) mutations in Pendred syndrome and nonsyndromic hearing loss associated with enlarged vestibular aqueduct: a unique spectrum of mutations in Japanese.** *Eur J Hum Genet* 2003, **11**:916–922.
16. Japanese Archipelago Human Population Genetics Consortium, Jinam T, Nishida N, Hirai M, Kawamura S, Oota H, Umetsu K, Kimura R, Ohashi J, Tajima A, Yamamoto T, Tanabe H, Mano S, Suto Y, Kaname T, Naritomi K, Yanagi K, Niikawa N, Omoto K, Tokunaga K, Saitou N: **The history of human populations in the Japanese Archipelago inferred from genome-wide SNP data with a special reference to the Ainu and the Ryukyuan populations.** *J Hum Genet* 2012, **57**:787–795.
17. Valvassori GE, Clemis JD: **The large vestibular aqueduct syndrome.** *Laryngoscope* 1978, **88**:723–728.
18. Phelps PD: **The basal turn of the cochlea.** *Br J Radiol* 1992, **65**:370–374.
19. Goldfeld M, Glaser B, Nassir E, Gomori JM, Hazani E, Bishara N: **CT of the ear in pendred syndrome.** *Radiology* 2005, **235**:537–540.
20. Davidson HC, Harnsberger HR, Lemmerling MM, Mancuso AA, White DK, Tong KA, Dahlen RT, Shelton C: **MR evaluation of vestibulocochlear anomalies associated with large endolymphatic duct and sac.** *AJNR Am J Neuroradiol* 1999, **20**:1435–1441.
21. Fraser GR: **Association of congenital deafness with goiter (Pendred's syndrome): a study of 207 families.** *Ann Hum Genet* 1965, **28**:201–249.
22. Valvassori GE: **The large vestibular aqueduct and associated anomalies of the inner ear.** *Otolaryngol Clin North Am* 1983, **16**:95–101.
23. Jackler RK, de la Cruz A: **The large vestibular aqueduct syndrome.** *Laryngoscope* 1989, **99**:1238–1243.
24. Levenson MJ, Parisier SC, Jacobs M, Edelstein DR: **The large vestibular aqueduct syndrome in children.** *Arch Otolaryngol Head Neck Surg* 1989, **115**:54–58.
25. Arcand P, Desrosiers M, Dube J, Abela A: **The large vestibular aqueduct syndrome and seisorineural hearing loss in the pediatric population.** *J Otolaryngol* 1991, **20**:247–250.
26. Belenky WM, Madgy DN, Leider JS, Becker C, Hotaling AJ: **The enlarged vestivular aqueduct syndrome (EVA syndrome).** *ENT J* 1993, **72**:746–751.
27. Okumura T, Takahashi H, Honjo I, Takagi A, Mitamura K: **Sensorineural hearing loss in patients with large vestibular aqueduct.** *Laryngoscope* 1995, **105**:289–294.
28. Stinckens C, Huygen PL, Joosten FB, Van Camp G, Otten B, Cremers CW: **Fluctuant, progressive hearing loss associated with Meniere like vertigo in three patients with the Pendred syndrome.** *Int J Pediatr Otorhinolaryngol* 2001, **61**:207–215.
29. Cremers CW, Admiraal RJ, Huygen PL, Bolder C, Everett LA, Joosten FB, Green ED, van Camp G, Otten BJ: **Progressive hearing loss, hypoplasia of the cochlea and widened vestibular aqueducts are very common features in Pendred's syndrome.** *Int J Pediatr Otorhinolaryngol* 1998, **45**:113–123.
30. Dossena S, Rodighiero S, Vezzoli V, Nofziger C, Salvioni E, Boccazzi M, Grabmayer E, Botta G, Meyer G, Fugazzola L, Beck-Peccoz P, Paulmichl M: **Functional characterization of wildtype and mutated pendrin (SLC26A4), the anion transporter involved in Pendred syndrome.** *J Mol Endocrinol* 2009, **43**:93–103.
31. Fugazzola L, Cerutti N, Mannavola D, Vannucchi G, Beck-Peccoz P: **The role of pendrin in iodide regulation.** *Exp Clin Endocr Diab* 2001, **109**:18–22.
32. Scott D, Wang R, Kreman T, Sheffield V, Karniski L: **The Pendred syndrome gene encodes a chloride-iodide transport protein.** *Nat Genet* 1999, **21**:440–443.
33. Scott DA, Wang R, Kreman TM, Andrews M, McDonald JM, Bishop JR, Smith RJH, Karnishki LP, Sheffield VC: **Functional differences of the PDS gene product are associated with phenotypic variation in patients with Pendred syndrome and non-syndromic hearing loss (DFNB4).** *Hum Mol Genet* 2000, **9**:1709–1715.
34. Reardon W, Coffey R, Chowdhury T, Grossman A, Jan H, Britton K, Kendall-Taylor P, Trembath R: **Prevalence, age of onset, and natural history of thyroid disease in Pendred syndrome.** *J Med Genet* 1999, **36**:595–598.
35. Napiontek U, Borck G, Muller-Forell W, Pfarr N, Bohnert A, Keilmann A, Pohlenz J: **Intrafamilial variability of the deafness and goiter phenotype in Pendred syndrome caused by a T416P mutation in the SLC26A4 gene.** *J Clin Endocrinol Metab* 2004, **89**:5347–5351.
36. Iwasaki S, Tsukamoto K, Usami S, Misawa K, Mizuta K, Mineta H: **Association of SLC26A4 mutation with clinical features and thyroid function in deaf infants with enlarged vestibular aqueduct.** *J Hum Genet* 2006, **51**:805–810.
37. Kitamura K, Takahashi K, Noguchi Y, Kuroishikawa Y, Tamagawa Y, Ishikawa K, Ichimura K, Hagiwara H: **Mutations of the Pendred syndrome gene (PDS) in patients with large vestibular aqueduct.** *Acta Otolaryngol* 2000, **120**:137–141.

38. Dai P, Li Q, Huang D, Yuan Y, Kang D, Miller DT, Shao H, Zhu Q, He J, Yu F, Liu X, Han B, Yuan H, Platt OS, Han D, Wu BL: **SLC26A4 c.919-2A > G varies among Chinese ethnic groups as a cause of hearing loss.** *Genet Med* 2008, **10**:586–592.
39. Chen K, Wang X, Sun L, Jiang H: **Screening of SLC26A4, FOXI1, KCNJ10, and GJB2 in bilateral deafness patients with inner ear malformation.** *Otolaryngol Head Neck Surg* 2012, **146**:972–978.
40. Wu CC, Yeh TH, Chen PJ, Hsu CJ: **Prevalent SLC26A4 mutations in patients with enlarged vestibular aqueduct and/or Mondini dysplasia: a unique spectrum of mutations in Taiwan, including a frequent founder mutation.** *Laryngoscope* 2005, **115**:1060–1064.
41. Shin JW, Lee SC, Lee HK, Park HJ: **Genetic screenig of GJB2 and SLC26A4 in Korean cochlear implantees: experience of soree Ear clinic.** *Clin Exp Otorhinolaryngol* 2012, **30**(Suppl 1):10–13.
42. Yang JJ, Tsai CC, Hsu HM, Shiao JY, Su CC, Li SY: **Hearing loss associated with enlarged vestibular aqueduct and Mondini dysplasia is caused by splice-site mutation in the PDS gene.** *Hear Res* 2005, **199**:22–30.
43. Wang QJ, Zhao YL, Rao SQ, Guo YF, Yuan H, Zong L, Guan J, Xu BC, Wang DY, Han MK, Lan L, Zhai SQ, Shen Y: **A distinct spectrum of SLC26A4 mutations in patients with enlarged vestibular aqueduct in China.** *Clin Genet* 2007, **72**:245–254.
44. Reyes S, Wang G, Ouyang X, Han B, Du LL, Yuan HJ, Yan D, Dai P, Liu XZ: **Mutation analysis of SLC26A4 in mainland Chinese patients with enlarged vestibular aqueduct.** *Otolaryngol Head Neck Surg* 2009, **141**:502–508.
45. Huang S, Han D, Yuan Y, Wang G, Kang D, Zhang X, Yan X, Meng X, Dong M, Dai P: **Extremely discrepant mutation spectrum of SLC26A4 between Chinese patients with isolated Mondini deformity and enlarged vestibular aqueduct.** *J Transl Med* 2011, **30**:167.
46. Krawczak M, Reiss J, Cooper DN: **The mutational spectrum of single base-pair substitutions in mRNA splice junctions of human genes: causes and consequences.** *Hum Genet* 1992, **90**:41–54.
47. Larriba S, Bassas L, Gimenez J, Ramos MD, Segura A, Nunes V, Estivill X, Casals T: **Testicular CFTR splice variants in patients with congenital absence of the vas deferens.** *Hum Mol Genet* 1998, **7**:1739–1744.
48. Betsalel OT, Rosenberg EH, Almeida LS, Kleefstra T, Schwartz CE, Valayannopoulos V, Abdul-Rahman O, Poplawski N, Vilarinho L, Wolf P, den Dunnen JT, Jakobs C, Salomons GS: **Characterization of novel SLC6A8 variants with the use of splice-site analysis tools and implementation of a newly developed LOVD database.** *Eur J Hum Genet* 2011, **19**:56–63.

doi:10.1186/1471-2350-14-56
Cite this article as: Ganaha *et al.*: Pathogenic substitution of IVS15 + 5G > A in *SLC26A4* in patients of Okinawa Islands with enlarged vestibular aqueduct syndrome or Pendred syndrome. *BMC Medical Genetics* 2013 14:56.

ORL

ORL 2013;75:342–349
DOI: 10.1159/000357474
Received: November 23, 2012
Accepted after revision: November 18, 2013
Published online: January 10, 2014

0301–1569/14/0756–0342$39.50/0
www.karger.com/orl

Original Paper

Glucose Metabolism in the Primary Auditory Cortex of Postlingually Deaf Patients: An FDG-PET Study

Takumi Okuda[a] Shigeki Nagamachi[b] Yasuaki Ushisako[a] Tetsuya Tono[a]

Departments of [a]Otolaryngology – Head and Neck Surgery and [b]Nuclear Medicine, Miyazaki University School of Medicine, Miyazaki, Japan

Key Words
FDG-PET · Neuroplasticity · Auditory cortex · Deafness

Abstract
Background/Purpose: Previous FDG-PET studies have indicated neuroplasticity in the adult auditory cortex in cases of postlingual deafness. In the mature brain, auditory deprivation decreased neuronal activity in primary auditory and auditory-related cortices. In order to re-evaluate these issues, we used statistical analytic software, namely a three-dimensional stereotaxic region of interest template (3DSRT), in addition to statistical parametric mapping (SPM; Institute of Neurology, University College of London, UK). ***Materials and Methods:*** ^{18}F-FDG brain PET scans were performed on 7 postlingually deaf patients and 10 healthy volunteers. Significant increases and decreases of regional cerebral glucose metabolism in the patient group were estimated by comparing their PET images with those of healthy volunteers using SPM analysis and 3DSRT. ***Results:*** SPM revealed that the glucose metabolism of the deaf patients was lower in the right superior temporal gyrus, both middle temporal gyri, left inferior temporal gyrus, right inferior lobulus parietalis, right posterior cingulate gyrus, and left insular cortex than that of the control subjects. 3DSRT data also revealed significantly decreased glucose metabolism in both primary auditory cortices of the postlingually deaf patients. ***Conclusion:*** SPM and 3DSRT analyses indicated that glucose metabolism decreased in the primary auditory cortex of the postlingually deaf patients. The previous results of PET studies were confirmed, and our method involving 3DSRT has proved to be useful.

Takumi Okuda
Department of Otolaryngology – Head and Neck Surgery
Miyazaki University School of Medicine
Kiyotakecho Kihara 5200, Miyazaki, Miyazaki 889-1692 (Japan)
E-Mail takumi_okuda@med.miyazaki-u.ac.jp

ORL 2013;75:342–349
DOI: 10.1159/000357474

Introduction

Previous FDG-PET studies have indicated neuroplasticity in the adult auditory cortex in cases of postlingual deafness. In the early 1990s, this phenomenon was discussed based on visual findings. In PET images, different colors indicate different rates of glucose metabolism. That is, red indicates a high rate, yellow a moderate, and blue a low rate [1]. Patient and normal control groups were compared in this way. Then, in the 2000s, a similar comparison was performed using voxel-based analysis software such as statistical parametric mapping (SPM; Institute of Neurology, University College of London, UK) [2]. SPM has been widely used for the objective analysis of brain images. This software package compares the differences between two anatomically standardized groups with the linear model at each voxel. However, it is sometimes not possible to detect slight differences because of technical issues. In the mature brain, auditory deprivation decreases neuronal activity transiently in the primary auditory and auditory-related cortices. In order to reevaluate these issues, we used a further statistical analytic software, namely a three-dimensional stereotaxic region of interest (ROI) template (3DSRT) [3], in addition to SPM. 3DSRT is fully automated ROI-based analysis software for the brain. It was established to perform ROI analysis of the brain with improved objectivity and excellent reproducibility [4–7].

Materials and Methods

In a resting state (eyes closed, ears unoccluded, dark and quiet environment), 185-MBq ^{18}F-FDG (the dose was adjusted according to the body weight of each subject) brain PET scans were performed on 7 postlingually deaf patients and 10 healthy volunteers using the Biograph 16 PET scanner (Siemens). Seven patients (2 men, 5 women; mean age, 55.7 ± 8.7 years) underwent FDG-PET scans at Miyazaki University Hospital between July 2012 and August 2013. The duration of deafness ranged from 1 to 30 years (mean duration, 13.4 ± 10.8). The clinical features of the patients are listed in table 1. They had neither cerebral disease nor visual disturbance. Ten age-matched healthy volunteers (2 men, 8 women; mean age, 57.9 ± 16.2 years) served as control subjects. Exclusion criteria for the control subjects included a history of any neurological, psychiatric or significant medical illness, or a history of drug abuse. All patients and control subjects were right-handed. Detailed explanations of the procedure, risk, and purpose of the FDG-PET study were provided to them. The present work was approved by the Ethics Committee of Miyazaki University School of Medicine, and written consent was obtained from each participant.

Significant increases and decreases of regional cerebral glucose metabolism in the patient group were estimated by comparing their FDG-PET images with those of the healthy volunteers using SPM analysis.

We also compared the glucose metabolism of auditory cortices with that of visual cortices using 3DSRT. Because all patients and control subjects had neither cerebral disease nor visual disturbances, we adopted the primary visual cortex as a reference. 3DSRT applies constant ROIs on anatomically standardized images and enables image analysis of miscellaneous radioactive tracers (^{99m}Tc-ECD, ^{123}I-IMP, [^{15}O]-H_2O, and ^{18}F-FDG) with excellent reproducibility and objectivity. The analytical process of this method is as follows: (1) anatomical standardization using the SPM algorithm; (2) analysis using 318 constant ROIs divided into 12 groups (segments) on each hemisphere; (3) calculation of the area-weighted average for each of the respective 24 segments based on the value in each ROI, and (4) display of the results followed by saving of the respective values of the 636 ROIs (both hemispheres) in the CSV file format. For 3DSRT analysis, 318 constant ROIs on each brain hemisphere were prepared. The constant ROIs were determined on the T1-weighted magnetic resonance images (MRI) anatomically standardized by SPM and classified into 12 segments according to their arterial supply. 3DSRT allows for quantitative analysis, in contrast to SPM, which involves statistical analysis.

Table 1. Clinical features of deaf patients

Patient No.	Age, years	Sex	Cause of deafness	Duration of deafness, years
1	50	F	Unknown	1
2	52	F	Unknown	24
3	63	F	Unknown	1
4	49	F	Head injury	30
5	47	M	Otosclerosis	13
6	72	M	Unknown	5
7	57	F	Unknown	20

Table 2. Significantly decreased glucose metabolism (deaf versus normal)

Region	Coordinates*			Analysis	
	x	y	z	Z**	p
Right middle temporal gyrus	43.6	−12.1	−8.6	3.67	0.001
Right inferior lobulus parietalis	23.8	−38.9	40.0	3.61	0.002
Right superior temporal gyrus	39.6	−2.2	−5.4	3.44	0.002
Right posterior cingulate gyrus	23.8	−39.1	37.0	3.61	0.003
Right posterior cingulate gyrus	23.8	−23.4	38.0	3.41	0.035
Left middle temporal gyrus	−41.6	−25.5	−4.3	3.35	0.008
Left inferior temporal gyrus	−35.6	−3.0	−20.1	3.29	0.009
Left insular cortex	−39.6	3.8	−2.03	3.09	0.011

* International Consortium on Brain Mapping coordinates for the location where the significant difference between conditions was centered.

** Z values refer to the comparison of normalized glucose metabolism between the deaf and the normal group.

Results

When we compared the ^{18}F-FDG brain PET images of the postlingually deaf patients with those of the healthy control subjects (fig. 1) by using the SPM method, the glucose metabolism of the deaf patients was lower in the right superior temporal gyrus, both middle temporal gyri, left inferior temporal gyrus, right inferior lobulus parietalis, right posterior cingulate gyrus, and left insular cortex (table 2). The 3DSRT data also revealed significantly decreased glucose metabolism in both primary auditory cortices of the postlingually deaf patients. We found a 13% decrease in the right hemisphere and a 16% decrease in the left hemisphere (fig. 2).

Discussion

Generally, cortical glucose metabolism in the sensory system characteristically decreases with sensory deficits, owing to the absence of central sensory input. The same pattern has been observed in the auditory system [8].

In the early 1990s, glucose metabolism in the auditory cortices was compared by PET on a visual basis. In PET images, different colors indicate different rates of glucose metabolism. That is, red indicates a high rate, yellow a moderate, and blue a low rate [1]. Since the early 2000s, SPM has been used for these studies [2]. Voxel-based analysis software such as SPM

ORL 2013;75:342–349
DOI: 10.1159/000357474

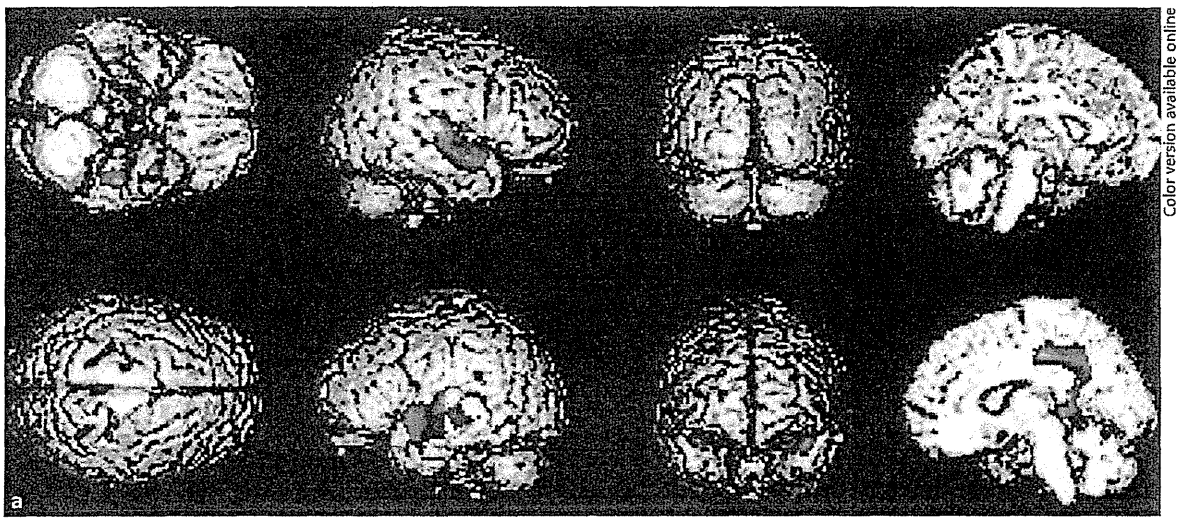

Color version available online

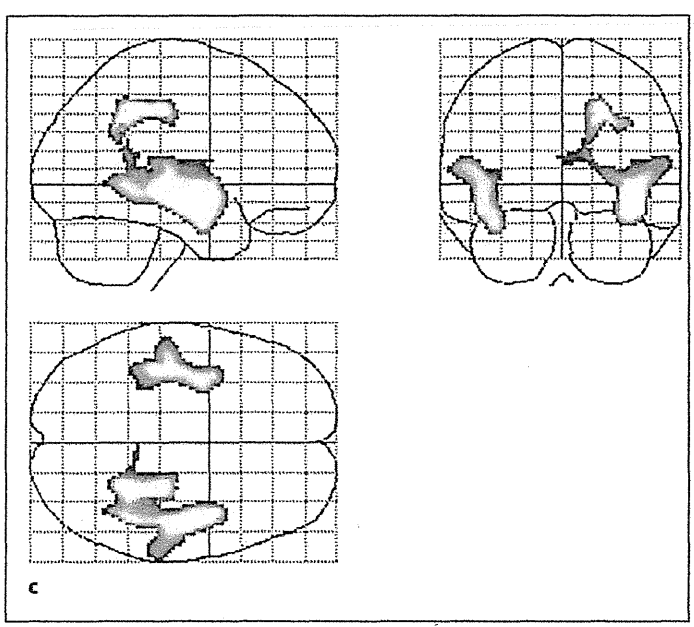

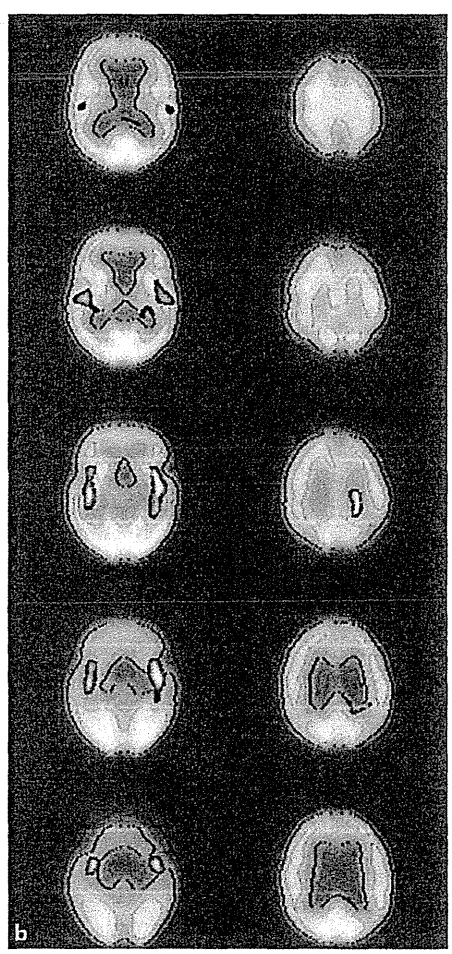

Fig. 1. Brain areas with significantly decreased glucose metabolism in the postlingually deaf patients ($p < 0.01$, uncorrected). Metabolism was decreased in the right superior temporal gyrus, inferior lobulus parietalis, posterior cingulate gyrus, and in both middle temporal gyri, the left inferior temporal gyrus as well as the insular cortex. **a** 3D volume-rendering image. **b** Axial image. **c** Maximum intensity projection.

ORL 2013;75:342–349
DOI: 10.1159/000357474

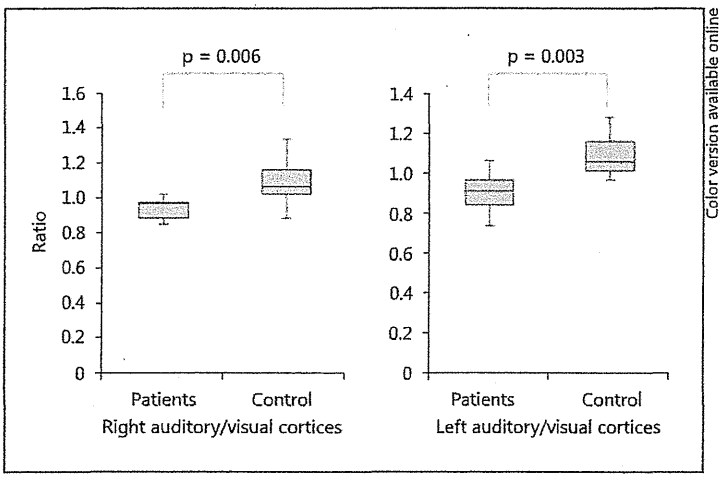

Fig. 2. 3DSRT data revealed significantly decreased glucose metabolism in both primary auditory cortices of the postlingually deaf patients.

has been widely used for the objective analysis of brain images with various imaging drugs. There are several reports about changes in the glucose uptake in the auditory cortex observed by FDG-PET.

In prelingually deaf children, the hypometabolic area of the auditory cortex was widest initially, but decreased as the duration of deafness increased. After 20 years of deafness, cortical glucose metabolism did not differ from that of normal controls [9]. This finding was supported by animal studies. In neonatal deafened rats, the same pattern was observed [10]. In addition, Lee et al. [9] found a positive correlation between the hearing performance of prelingually deafened children after cochlear implantation and the extent of the preoperative hypometabolic area in the auditory cortex. Glucose metabolism in the temporal lobe of deaf children increases with age, and the hearing outcomes deteriorate accordingly. We consider that this phenomenon involves the cross-modal plasticity of the brain. Because of the long-term absence of auditory input in congenitally deaf children, the auditory cortex is gradually displaced for another sensory center. Therefore, as the child grows older and the duration of deafness increases, the hearing-capability score with a cochlear implant gets worse. An FDG-PET study before cochlear implantation can predict the prognosis for prelingually deaf children.

Indeed, there are some reports of visual language activation studies by FDG-PET describing that the auditory association area of a deaf child develops to process visual aspects of language if it does not receive sufficient auditory signals in the developmental period. In addition, this cross-modal plasticity is suppressed and replaced by normal development if the child uses a hearing prosthesis such as a hearing aid or a cochlear implant to increase his or her spoken language skills [11, 12].

This fact was confirmed by other methods such as magnetoencephalography or functional MRI. Levänen et al. [13] reported that vibrotactile stimuli, applied on the palm and fingers of a congenitally deaf adult, activated his/her auditory cortices. The recorded magnetoencephalography signals also indicated that the auditory cortices could discriminate between the applied 180- and 250-Hz vibration frequencies. Similar to the visual language activation study by FDG-PET, these findings suggest that human cortical areas, normally subserving hearing, may process vibrotactile information in the congenitally deaf because of the lack of auditory signals. Sadato et al. [14] used functional MRI to study prelingually deaf signers, hearing non-signers, and hearing signers. The visually presented tasks included mouth-movement matching, random-dot motion matching, and sign-related motion matching.

ORL 2013;75:342–349
DOI: 10.1159/000357474

During the mouth-movement matching tasks, the deaf subjects showed more prominent activation of the left planum temporale than the hearing individuals. During dot-motion matching, the deaf showed greater activation in the right planum temporale. These findings suggest that cross-modal plasticity is induced by auditory deprivation independent of the lexical processes or visual phonetics, and this plasticity is mediated in part by the neural substrates of audio-visual cross-modal integration.

These facts constitute evidence that the operation of a cochlear implant for prelingually deaf children should be started as early as possible.

First, however, it has to be determined whether there really is a positive correlation between the degree of hypometabolism and a good cochlear implant outcome in postlingually deaf patients. If such a correlation is confirmed, an FDG-PET study before cochlear implantation can predict the prognosis not only for prelingually deaf children but also for postlingually deaf patients.

Initially, we estimated the auditory cortical glucose metabolism of the postlingually deaf patients at our hospital, using SPM analysis. The result was the same as reported by previous studies, namely low glucose metabolism in the auditory-related cortices of the postlingually deaf patients.

Incidentally, in postlingual human deafness, metabolism in the auditory cortex was significantly decreased after long-term deafness [2]. Ito et al. [1] described that the glucose metabolic rate in the auditory cortex of patients who have been deaf for a short period is nearly normal or slightly decreased. On the other hand, patients who have been deaf for a long time show decreased activity in the auditory cortex. If the period of deafness is long, e.g., over 10 years, the primary auditory cortex as well as the secondary associated cortex will exhibit a low glucose metabolic rate [1]. Similarly, in postlingual human deafness, glucose metabolism in the auditory cortex was found to be significantly decreased after 8 years of deafness [2]. We assume that the ability for cross-modal plasticity declines with age.

However, it has been reported that in adult deaf animals, metabolism in the auditory cortex returns. In adult deafened cats, glucose metabolism was significantly reduced bilaterally in the primary auditory cortex and the temporal auditory fields 4 months after the induction of deafness. Eventually, after 33 months, these changes disappeared [15]. Cross-modal plasticity of adult animals may differ from that of humans. Alternatively, this difference may result from the use of statistical tools such as SPM.

SPM is a program developed for the analysis of functional images of the human brain. Caution is advised in the use and selection of controls when utilizing SPM [16], and also when considering the results of reports because there are some previous FDG-PET studies that compared the brains of prelingually deafened children with those of a control group of normal-hearing adults by a t test in the basic model of SPM [9, 11]. Analysis should be performed under age-matched conditions, and sufficient numbers of control subjects are needed to ensure the validity of the obtained results. In addition, when controls are selected, only subjects judged to be healthy after a careful neurological examination should be included. Occasionally, there are some regions showing a decrease of regional cerebral glucose metabolism in SPM analysis that is not statistically significant, while other regions show only a minor difference that becomes significant, however.

Our method involving 3DSRT aimed to overcome these faults of SPM. SPM was effective for the statistical analysis of regional cerebral blood flow (rCBF) changes, but a lack of suitability for the quantification of rCBF values was noted owing to the positioning or selection of the ROI, an essential step for the quantification of brain images. As long as ROIs were manually selected, the obtained results fluctuated considerably with subtle changes in their positioning, and it was possible to overlook important information in an area in which ROI had not been set. Caution should also be taken with regard to SPM in that it is impossible to

evaluate the rCBF when the blood flow of the whole brain is decreased. In cases with a high-blood-flow area, the normal-blood-flow area will be considered to exhibit a low blood flow, leading to erroneous results.

To perform ROI analysis of the brain with improved objectivity and excellent reproducibility, 3DSRT, which is fully automated ROI-based analysis software for the brain, was established [3]. In quantifying rCBF or cerebral glucose metabolism, the radiological activity count cannot be adapted directly from 3DSRT. Among other things, this limitation is due to differences in blood volume or in radioisotope (RI) doses between individuals. However, in quantifying rCBF by using SPECT, simple procedures such as the Patlak plot method are available [17], allowing for direct rCBF comparison between individuals. For measuring brain glucose metabolism using FDG-PET, however, the procedure is complicated and invasive. Therefore, we used the RI count ratio as a reference region in the semi-quantitative method. Thereby, we set the primary visual cortex as the reference region and compared the RI count ratios of the primary auditory cortex and the primary visual cortex between the cases. None of the patients and control subjects had a cerebral disease or visual disturbances. Using the newly developed method, we could compare the cerebral glucose metabolism between the patients statistically. In addition, the previous results of FDG-PET study were confirmed.

Setting the primary visual cortex as the reference region and comparing the RI count ratios of the primary auditory cortex and the primary visual cortex from 3DSRT between the patient and control groups has proved to be a useful method. In contrast to SPM, which involves statistical analysis, our method allows for quantitative analysis and indicates the ratio of difference. Our data showed that glucose metabolism decreased in the primary auditory cortex of the postlingually deaf patients, with a duration of deafness in patients ranging from 1 to 30 years.

Additional effort is necessary to overcome the weaknesses of SPM. SPM requires spatial normalization to align all images to a standard anatomic model (the template), but this may lead to image distortion and artifacts, especially in cases of marked brain abnormalities. Person et al. [18] aimed to assess a block-matching normalization algorithm in which most transformations are not directly computed on the overall brain volume but through small blocks, a principle that is likely to minimize artifacts.

Conclusion

The two statistical tools indicated that glucose metabolism decreased in the primary auditory cortex of the postlingually deaf patients. Our results show the same pattern as described in previous reports. Our method involving 3DSRT has proved to be useful as it enabled us to perform quantitative analysis and can indicate the ratio of difference.

Functional brain imaging is an indirect assessment that evaluates the cortical activity by rCBF or metabolic changes. Moreover, the assessment requires reasonable number of control subjects. In view of the obtained results, we should keep this in mind at all times.

For determining whether an FDG-PET study before cochlear implantation will contribute to predict prognosis, high numbers of study participants, individual comparison of patients and controls, and detailed evaluation of the correlation between the degree of auditory cortical hypometabolism and a good cochlear implant outcome are needed.

ORL 2013;75:342–349
DOI: 10.1159/000357474

References

1 Ito J, Sakakibara J, Iwasaki Y, Yonekura Y: Positron emission computed tomography of auditory sensation in deaf patients and patients with cochlear implants. Ann Otol Rhinol Laryngol 1993;102:797–801.
2 Lee JS, Lee DS, Oh SH, Kim CS, Kim JW, Hwang CH, Koo J, Kang E, Chung JK, Lee MC: PET evidence of neuroplasticity in adult auditory cortex of postlingual deafness. J Nucl Med 2003;44:1435–1439.
3 Takeuchi R, Sengoku T, Matsumura K: Usefulness of fully automated constant ROI analysis software for the brain: 3DSRT and FineSRT. Radiat Med 2006;24:538–544.
4 Tateno M, Utsumi K, Kobayashi S, Takahashi A, Saitoh M, Morii H, Fujii K, Teraoka M: Usefulness of a blood flow analyzing program 3DSRT to detect occipital hypoperfusion in dementia with Lewy bodies. Prog Neuropsychopharmacol Biol Psychiatry 2008;32:1206–1209.
5 Kataoka K, Hashimoto H, Kawabe J, Higashiyama S, Akiyama H, Shimada A, Kai T, Inoue K, Shiomi S, Kiriike N: Frontal hypoperfusion in depressed patients with dementia of Alzheimer type demonstrated on 3DSRT. Psychiatry Clin Neurosci 2010;64:293–298.
6 Torigai T, Mase M, Ohno T, Katano H, Nisikawa Y, Sakurai K, Sasaki S, Toyama J, Yamada K: Usefulness of dual and fully automated measurements of cerebral blood flow during balloon occlusion test of the internal carotid artery. J Stroke Cerebrovasc Dis 2011;17:1–8.
7 Marushima A, Tsurushima H, Suzuki K, Nakai Y, Nemoto H, Matsumura A: Time-course analysis of brain perfusion single photon emission computed tomography using a three dimensional stereotactic region-of-interest template in patients with moyamoya disease. World Neurosurg 2011;76:304–310.
8 Rauschecker JP: Auditory cortical plasticity: a comparison with other sensory systems. Trends Neurosci 1999; 22:74–80.
9 Lee DS, Lee JS, Oh SH, Kim SK, Kim JW, Chung JK, Lee MC, Kim CS: Cross-modal plasticity and cochlear implants. Nature 2001;409:149–150.
10 Ahn SH, Oh SH, Lee JS, Jeong JM, Lim D, Lee DS, Kim CS: Changes of 2-deoxyglucose uptake in the rat auditory pathway after bilateral ablation of the cochlea. Hear Res 2004;196:33–38.
11 Fujiwara K, Naito Y, Senda M, Mori T, Manabe T, Shinohara S, Kikuchi M, Hori SY, Tona Y, Yamazaki H: Brain metabolism of children with profound deafness: a visual language activation study by 18F-fluorodeoxyglucose positron emission tomography. Acta Otolaryngol 2008;128:393–397.
12 Moteki H, Naito Y, Fujiwara K, Kitoh R, Nishio SY, Oguchi K, Takumi Y, Usami S: Different cortical metabolic activation by visual stimuli possibly due to different time courses of hearing loss in patients with GJB2 and SLC26A4 mutations. Acta Otolaryngol 2011;131:1232–1236.
13 Levänen S, Jousmäki V, Hari R: Vibration-induced auditory-cortex activation in a congenitally deaf adult. Curr Biol 1998;8:869–872.
14 Sadato N, Okada T, Honda M, Matsuki K, Yoshida M, Kashikura K, Takei W, Sato T, Kochiyama T, Yonekura Y: Cross-modal integration and plastic changes revealed by lip movement, random-dot motion and sign languages in the hearing and deaf. Cereb Cortex 2005;15:1113–1122.
15 Park MH, Lee HJ, Kim JS, Lee JS, Lee DS, Oh SH: Cross-modal and compensatory plasticity in adult deafened cats: a longitudinal PET study. Brain Res 2010;1354:85–90.
16 Schwartzman A, Dougherty RF, Lee J, Ghahremani D, Taylor JE: Empirical null and false discovery rate analysis in neuroimaging. Neuroimage 2009;44:71–82.
17 Lawson RS: Application of mathematical methods in dynamic nuclear medicine studies. Phys Med Biol 1999; 44:R57–R98.
18 Person C, Louis-Dorr V, Poussier S, Commowick O, Malandain G, Maillard L, Wolf D, Gillet N, Roch V, Karcher G, Marie PY: Voxel-based quantitative analysis of brain images from ^{18}F-FDG PET with a block-matching algorithm for spatial normalization. Clin Nucl Med 2012;37:268–273.

Otol Jpn 23(3): 238-242, 2013

コンビームCTによる蝸牛窓臨床解剖の検討

中島　崇博*、東野　哲也**、奥田　匠**、松田　圭二**、髙木　実*、
林　多聞*、花牟禮　豊*
*鹿児島市立病院　耳鼻咽喉科
**宮崎大学　医学部　耳鼻咽喉・頭頸部外科

Evaluation of the clinical anatomy of the round window membrane using cone-beam computed tomography (CBCT)

Takahiro Nakashima *, Tetsuya Tono **, Takumi Okuda **, Keiji Matsuda **, Minoru Takaki *, Tamon Hayashi *, Yutaka Hanamure *
* Department of Otolaryngology-Head and Neck Surgery, Kagoshima City Hospital
** Department of Otolaryngology-Head and Neck Surgery, University of Miyazaki

Understanding the clinical anatomy of the round window membrane (RWM) is important in the era of implantable hearing devices. Cone-beam computed tomography (CBCT) is used for the evaluation of the temporal bone. The quality of the image obtained by CBCT is almost equal to that of high resolution computed tomography. The purpose of this study was to confirm the efficacy of CBCT for the measurement and evaluation of the round window membrane.

Fifty ears from 37 patients that underwent CBCT in Kagoshima City Hospital, which had well pneumatized mesotympanum, were selected. The width of the RWM was measured in an axial view. Angle A and B were defined in order to evaluate the surgical approach to the round window niche (RWN) and RWM. A tangent to the facial canal through the roof of RWN, a line through the floor of RWN and the base of suprameatal spine, and a tangent to the RWM were defined to be lines a, b, and c, respectively. The acute angle between line a and line b was angle A, and that between line b and line c was angle B.

The diameter of the RWM, angle A, and angle B were approximately 1.55 mm, 25.7 degrees, and 31.5 degrees, respectively. A statistical analysis showed that none of these data had any correlation with the age or gender.

These data were consistent with that reported in the literature, in which the distance was measured by histological procedures. The figure showed that angle A indicated the range for the opening the facial recess by a posterior tympanotomy and angle B indicated the range of the direction to the RWM. The data indicated that the direction from which the surgeon could completely identify the RWN and RWM was relatively limited and the RWM could not be observed from an oblique direction. Preoperative CBCT provided the surgeon with useful information for ear surgery, especially for placing a cochlear implant.

Key words：flat panel detector, round window niche, posterior tympanotomy
和文キーワード：フラットパネルディテクタ，蝸牛窓小窩，後鼓室開放術

論文要旨

近年の植込み型人工聴覚器医療の展開に伴い、蝸牛窓周辺の臨床解剖の重要性が増している。

鹿児島市立病院にてCBCTを施行した37症例50耳を対象とし、再構築画像にて蝸牛窓径を計測したところ、蝸牛窓径は1.55mmであった。また、蝸牛窓小窩のroof

から顔面神経管への接線（a）、道上棘基部と蝸牛窓小窩底部を結ぶ直線（b）、および蝸牛窓の接線（c）を設定し、直線（a）（b）及び（b）（c）がなす角度をそれぞれ角A、Bとすると、角Aは25.7°、角Bは31.5°であった。

蝸牛窓径は過去の組織学的検討とほぼ同様であった。角Aは乳突削開後後鼓室開放した際に蝸牛窓を確認できる範囲、角Bは道上棘付近からみた蝸牛窓面の角度ととらえられる。蝸牛窓全景を確認する方向は限定されること、蝸牛窓は術者の視軸に対して斜めに確認されること、何れも個人差が大きいことがわかった。CBCTは蝸牛窓に対する有用な術前評価方法と思われた。

はじめに

低音域聴力残存症例に対して、cochleostomy insertionよりもround window insertionを選択することで、人工内耳電極挿入後の低音域聴力が温存されることが示されている[1]。また、vibrant sound bridgeにおけるround window vibroplasty[2]など、蝸牛窓周囲の臨床解剖の理解は重要性を増している。術前検査としての高分解能CTは今や耳科手術において必須であるが、的確な再構築画像を得るためには、側頭骨解剖に習熟した放射線科医の介入が不可欠である。一方で、ここ数年耳鼻咽喉科領域での有用性が報告されているコンビームCT（以下CBCT）は、比較的簡単な設定と操作で高分解能CTに劣らない細密な画像が得られ、任意のスライスを簡単に表示出来るだけでなく、3次元画像も容易に作成できる。今回我々は術前の蝸牛窓周囲の評価におけるCBCTの有用性を検討すべく、蝸牛窓径、および後鼓室開放術における蝸牛窓術野についての計測を行なった。

対象と方法

2012年1月から4月までの間に鹿児島市立病院耳鼻咽喉科にてCBCTを施行した66例131耳のうち、蝸牛窓周囲に軟部組織陰影がない37例50耳を対象とした。男性16例21耳、女性21例29耳、年齢は9歳から78歳であった（図1）。疾患は、真珠腫（術後耳、外耳道真珠腫を含む）15耳、慢性中耳炎（術後耳を含む）14耳、難聴（伝音、感音あるいは混合性難聴の精査）8耳、めまい（メニエール、外リンパ瘻含む）8耳、耳鳴症4耳、外傷性鼓膜穿孔1耳であった。真珠腫例と慢性中耳炎例29耳については、健側耳、あるいは患側耳でも画像上中鼓室に軟部組織陰影の無い耳を選択したため、50耳中43耳は非炎症耳で、慢性炎症耳は7耳となった。

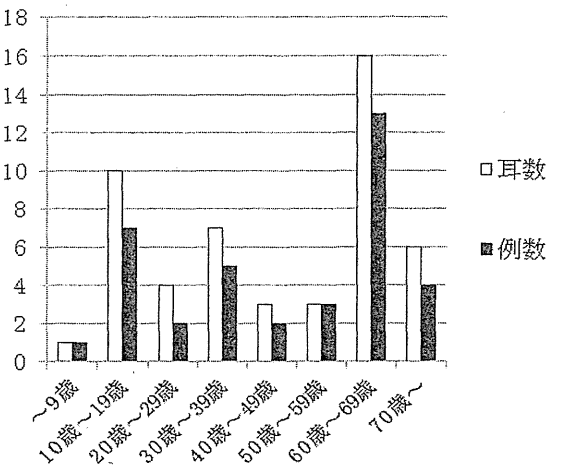

図1　年齢分布

縦軸に耳数（白）および例数（黒）、横軸に年代をとり棒グラフを示す。

CBCTはモリタ製作所の3D Accu-i-tomo F17®を用いた。撮影は座位で施行し、ヘッドレスト、ヘッドバンドとチンレストで頭部を固定して水平面が概ねOM line－30°となるようにした。管電圧は90kV、管電流は8mAとし、撮影時間は17.5秒、360°回転して得られた578枚の撮像データを付属ソフト（i-View®）で再構成し、軸位断、前額断、矢状断の3方向の再構築画像を得た。関心領域は60×60mm、ボクセルサイズは0.125mmとした。

軸位断にて道上棘、顔面神経管、蝸牛基底回転、蝸牛窓小窩を同定し、蝸牛窓小窩の含気腔と蝸牛基底回転との境界線の長さを蝸牛窓径として計測した（図2①）。次に、蝸牛窓小窩のroofから顔面神経管への接線（a）、および道上棘基部から顔面神経管を接して蝸牛窓小窩の底部に至る直線（b）を設定した。これは、乳突削開術に続いて後鼓室開放術を施行した際に、手術用顕微鏡下で顔面神経管越しに蝸牛窓小窩を観察しうる視軸の範囲を示している。よって、この2本の直線の挟角Aは、後鼓室を開放した術野から蝸牛窓小窩を観察しうる範囲ととらえられ、この角度を計測した（図2②）。さらに、蝸牛窓面に対する接線（c）を設定した。前述の直線（b）と接線（c）のなす挟角Bは蝸牛窓全景を術野から見た際の、道上棘付近から見た蝸牛窓面の角度ととらえられ、この角度を計測した（図2③）。

以上の3項目について、それぞれの計測値と、年齢、性別との間の相関関係について統計学的検討を行なった。計測値と年齢についてはスペアマン順位相関検定、計測値と性別についてはマンホイットニー順位和検定を

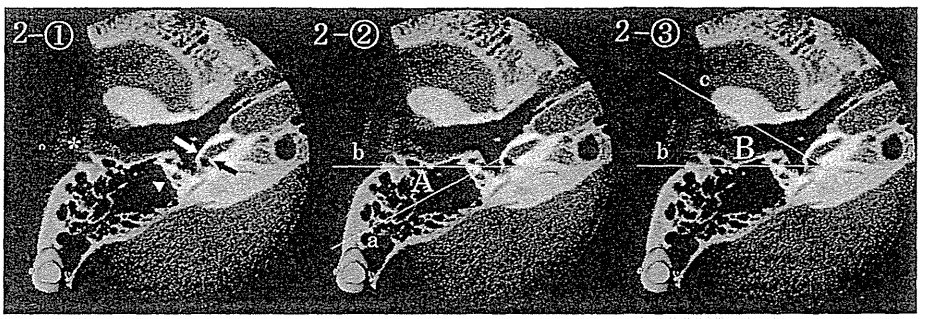

図2　右側頭骨軸位CBCT画像における蝸牛窓解剖の計測法

①：道上棘（*）、顔面神経管（矢頭）、蝸牛窓（向かい合う矢印の間）。②：直線aおよびbとその挟角Aを示す。③：直線bおよびcとその挟角Bを示す。

用いた。

結　果

蝸牛窓径は1.23mmから1.96mmで、中央値1.55mmであった。角度Aは13.3°から39.6°で、中央値は25.7°であった。また、角度Bは15.3°から44.9°、中央値は31.5°であった（図3、4、5）。個々のデータ分布と箱ひげ図が示すようにデータのばらつきが認められた。計測値と年齢については、今回の対象年齢において統計学的に相関関係は認めなかった。性差については、蝸牛窓径、角Aおよび角Bの中央値は男性、女性の順にそれぞれ1.56mmと1.54mm、26.1°と25.7°、および32.4°と30.9°であった。統計学的検定にて有意差を認めなかった。

考　察

蝸牛窓の臨床解剖学的検討は多くはないが、すでに詳細な報告がある。Proctorら[3]は蝸牛窓小窩について、計測値などのデータはないものの、発生学的見地も交え

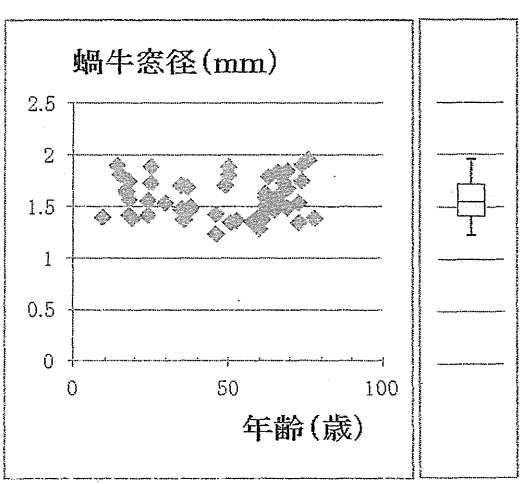

図3　蝸牛窓径の測定値およびその箱ひげ図

縦軸に測定値（mm）、横軸に年齢（歳）をとり実測値をプロットした（図左側）。また、その箱ひげ図を表示した（図右側）。

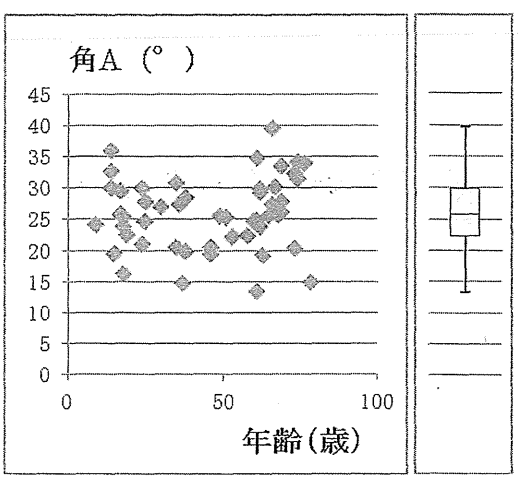

図4　角Aの測定値およびその箱ひげ図

縦軸に測定値（°）、横軸に年齢（歳）をとり実測値をプロットした（図左側）。また、その箱ひげ図を表示した（図右側）。

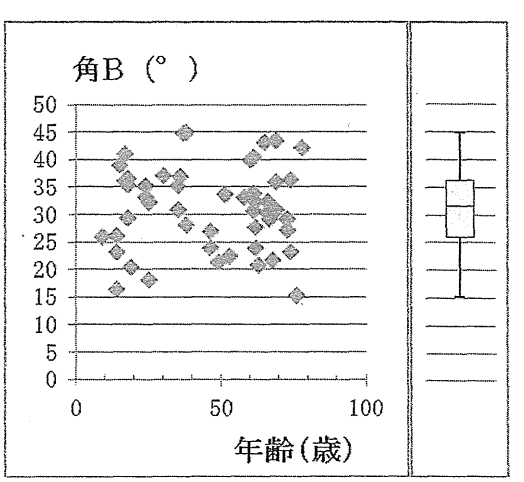

図5　角Bの測定値およびその箱ひげ図

縦軸に測定値（°）、横軸に年齢（歳）をとり実測値をプロットした（図左側）。また、その箱ひげ図を表示した（図右側）。

て詳しく記載している。Suら[4]は組織学的に蝸牛窓径を計測しており、年齢世代に関係なく1.65mmと報告している。Takahashiら[5]は組織学的計測結果をコンピューター解析することで3D画像を作成し、蝸牛窓面の細かな形状まで再現したうえで、その長径を1.76±0.10mmと報告している。

一方、CBCTについては近年基礎的臨床的研究報告が年々増加している。Guptaら[6]は側頭骨内の42項目の微小構造について、点数化してmultisection CTとの比較検討を行ない、CBCTが有意に良かったとしている。ただしここで用いられたCBCTはプロトタイプで、管電流、管電圧とも高く設定され、スライス数も900に上る。現在流通しているCBCTの撮影条件での検討ではないが、開発の時点ですでに従来のマルチスライスCTより側頭骨微小構造の描出が向上する可能性に注目していることがわかる。その後もin vitroおよびin vivo両面で人工耳小骨の評価や人工内耳の電極の評価に関する報告[7)~10)]がなされており、CBCTによる構築画像は、側頭骨の微細構造を十分に描出できると考えられる。

CBCTの濃度レベルは基準を設定しない相対値であり、CT値による計測点の定義ができないため、本検討では目測による計測を行なった。よって、目測による誤差およびpartial volume effectによる誤差を考慮しなければならない。これらをそれぞれ最少の1ボクセルとしても、誤差は少なくとも2ボクセル、すなわち0.25mmを見積もる必要がある。本検討では平均値±SDは1.58±0.19であった。前述のSuらの報告[4]は1.65±0.21で、組織学的計測値に近い値となった。画像による簡便な計測であるが、計測誤差は2ボクセル未満に抑えられていると思われ、耳科手術の術前検査として十分な精度と正確性を担保していると思われた。

CBCTの利点の一つに、比較的容易に3D画像を構築できることが挙げられる。この再構築画像は任意のスライスで長さや角度の計測が可能である。この機能を利用して、術野に関する画像的考察をすべく、方法の部分で述べたような角度の計測を行なった。乳突削開術後に後鼓室開放術を施行した際に、顔面神経管越しに蝸牛窓小窩のroof部分から蝸牛窓下端まで確認できる範囲が、角Aととらえられる。実際の手術ではこの角度の範囲内で出来るだけ蝸牛窓全景を明視下にしつつ手術を施行することになるため、視軸の位置は角Aのほぼ中央付近で操作することが多いと思われる。人工内耳手術においては、後鼓室開放術にてfacial recessを開放した後、cochleostomy insertionを施行する際、蝸牛窓小窩のroof部分を術野の中心にして、蝸牛窓より前下方に開窓する。通常facial recessは2mm以上の幅を以って開放可能で、roofの部分は確認し易い。しかし、時に顔面神経管を極めて薄く削っても蝸牛窓小窩全景を確認するのが困難な例に遭遇することがある。計測値は13.3°から39.6°とバリエーションが大きい。角Aが小さいほど、限られた方向からしか蝸牛窓小窩の観察ができないことになり、人工内耳手術において注意が必要と思われる。残存聴力活用型人工内耳ではround window insertionが好ましいとする報告[11)]もあるが、解剖学的制約からcochleostomy insertionを選択せざるを得ない場合を想定して手術に臨む準備が必要かもしれない。

角Bは道上棘付近から見た蝸牛窓面のなす角度である。人工内耳手術において、蝸牛窓を同定して電極を挿入する方向は、道上棘からの方向よりも後方尾側寄りになる。蝸牛窓面に対する挿入角度を正確に計測するには3次元的計測が必要となるため、角Bはこの挿入角度ととらえることは出来ない。しかしながら、角Bは軸位断で簡便に計測可能であり、術前に実際の挿入角度を想定する参考値としての臨床的意義があると思われる。例えば、角Bが大きいほど電極挿入方向に対する蝸牛窓面の成す角度も大きく、より蝸牛窓を観察しやすいことが想定される。これはround window insertionをする上では有利な情報である。蝸牛窓面の計測と人工内耳電極の挿入角度については、すでにTakahashiら[12)]が、蝸牛窓面を組織学的計測値からコンピューター解析し、蝸牛窓面に対する人工内耳電極挿入角度を31.9±3.6°と算出している。角Bは31.5°で比較的近似しており、参考値としての活用は有用かもしれない。いずれの角度にしろ、蝸牛窓を斜めから観察せざるを得ない解剖学的制約を数値的に示しており、蝸牛窓の露出には蝸牛窓小窩のroofおよびlipを必要十分に切削することが肝要であることが改めて認識された。また、角A同様、15.3°から44.9°と個人差が大きい。加えて、蝸牛窓小窩のroofや前後のlipの形状にも若干の個人差があり、実際の切削においてCBCTの術前評価で得られるデータの有用性は高いと思われる。

計測値と年齢について、結果は相関関係なしであった。しかし、CBCTは座位で施行するため、低年齢の小児は撮影自体困難な場合が多く、対象には若年小児例が含まれていない。蝸牛窓径については、Suら[4]が乳幼児についても他の年代と差がないことを報告しているが、角度の計測については、乳突蜂巣の発育途上の若年小児例では他の年代とは異なる傾向を示す可能性がある。乳幼

児のCBCTによる評価は不可能であるが、撮影可能な小児に限定すれば、角度と年齢との間に何らかの関連性が認められるかもしれない。

人工内耳適応の拡大、インプラントの改良、低音域の聴力残存型に対する低侵襲手術など、人工内耳医療の進歩に伴い、電極挿入部分の臨床解剖の知識はさらに重要性を増すと考えられる。今回の対象には人工内耳手術施行例や適応症例は含まれていなかったが、人工内耳手術施行にあたり、CBCTによる術前評価は、電極挿入の難易度を想定するうえで、ある程度客観的で有益なデータを術者に提供しうるものと思われた。

ま と め

CBCTによる蝸牛窓周囲の臨床解剖を、とくに人工内耳手術の観点から評価した。蝸牛窓径については過去の組織学的データと概ね同様の値となり、妥当な値と思われた。蝸牛窓小窩および蝸牛窓面に関して、術野に関する独自の角度を設定し計測したところ、年齢性別に関係なく個人差が大きいことが示された。CBCTによる術前評価により、後鼓室開放術、人工内耳手術における内耳開窓および電極挿入の難易度の想定において、術者は有益な術前情報を得られると思われた。

本論文の要旨は2012年10月第22回日本耳科学会総会学術講演会（名古屋）にて口演した。

参考文献

1）Skarzynski H, Lorens A, Piotrowska A, et al.：Preservation of low frequency hearing in partial deafness cochlear implantation (PDCI) using the round window surgical approach. Acta Oto-Laryngol 127：41–48, 2007.
2）Sainoo Y, Takahashi H, Kumagami H, et al.：Japanese experiences of the Vibrant Soundbridge-Round window application. Pract Otol (Kyoto) Suppl 132：78–83, 2012.
3）Proctor B, Bollobas B, Niparko JK：Anatomy of the round window niche. Ann Otol Rhinol Laryngol 95：444–446, 1986.
4）Su WY, Marion MS, Hinojosa R, et al.：Anatomical measurements of the cochlear aqueduct, round window membrane, round window niche, and facial recess. Laryngoscope 92：483–486, 1982.
5）Takahashi H, Takagi A, Sando I：Computer-aided three dimensional reconstruction and measurement of the round window and its membrane. Otolaryngol Head Neck Surg 101：517–521, 1989.
6）Gupta R, Bartling SH, Basu SK, et al.：Experimental flat-panel high-spatial-resolution volume CT of the temporal bone. AJNR 25：1417–1424, 2004.
7）Monteiro E, Das P, Daly M, et al.：Usefulness of cone-beam computed tomography in determining the position of ossicular prostheses: a cadaveric model. Otol Neurotol 32：1358–1363, 2011.
8）Komori M, Yanagihara N, Hyodo J, et al.：Position of TORP of the stapes footplate assessed with cone beam computed tomography. Otol Neurotol 33：1353–1356, 2012.
9）Husstedt HW, Aschendorff A, Richter B, et al.：Nondestructive three-dimensional analysis of electrode to modiolus proximity. Otol Neurotol 23：49–52, 2002.
10）Trieger A, Schulze A, Schneider M, et al.：In vivo measurements of the insertion depth of cochlear implant arrays using flat-panel volume computed tomography. Otol Neurotol 32：152–157, 2010.
11）Usami S, Moteki H, Suzuki N, et al.：Achievement of hearing preservation in the presence of an electrode covering the residual hearing region. Acta Otolaryngol 131：405–412, 2011.
12）Takahashi H, Sando I：Computer-aided 3-D temporal bone anatomy for cochlear implant surgery. Laryngoscope 100：417–421, 1990.

論文受付　25年3月11日
論文受理　25年5月4日

別刷請求先：〒892-0846　鹿児島県鹿児島市加治屋町20-17
鹿児島市立病院 耳鼻咽喉科　中島　崇博